Evaluation of Supernova Data Without Cosmic Acceleration Using a Three Parameter Redshift Model - Shining Light on Dark Energy

Tracy McSheery tracymc@phasespace.com

Abstract

We present a statistical validation of a supernova model on 4,831 Type Ia supernovae from the DES-SN5YR compilation. The model posits that observed redshift–brightness relations are governed by local photon-interaction physics—a multi-component mechanism—rather than cosmic acceleration. The model is parameterized by three physical couplings: a baseline “drag” kernel (k_J), a non-linear flux-dependent scattering term (η′), and a near-source saturation factor (ξ). Using a vectorized JAX/NumPyro MCMC fitter with a Student-t likelihood, we obtain well-mixed posteriors ($\hat{R}$ = 1.00, effective sample size > 10,000, zero divergences). The curve reproduces the Hubble diagram with flat median residuals versus redshift and an overall RMS of ≈ 1.89 mag under a common A→μ mapping. This RMS reflects the total population variance before applying the empirical color and light-curve shape corrections common in standard cosmological analyses, as the goal of this study is to test the model's ability to reproduce the global Hubble trend from a minimal set of physical principles. An A/B/C model comparison (unconstrained; sign-constrained; orthogonalized basis) shows the unconstrained model achieves the best information criteria and convergence, indicating that mild collinearity of the basis functions is informative rather than pathological. A deliberately adverse holdout set (objects failing Stage-1 per-SN fit screening) exhibits substantially larger dispersion, consistent with out-of-distribution conditions rather than overfitting. These results show that the foundational supernova evidence for Dark Energy can be explained by local, near-source photon physics. We outline falsifiable follow-ups using color and time-domain temperature markers to break remaining degeneracies.

Keywords: Type Ia supernovae, Hubble diagram, Quantum Field Dynamics, photon transport, flux-dependent redshift, NumPyro, static-universe interpretation

1. Introduction

The standard ΛCDM interpretation of the supernova Hubble diagram invokes an accelerating expansion driven by a dark-energy component. While successful in many respects, this framework faces tensions and relies on physics not verified in the laboratory and achieves the fit by selecting data. This Model offers an alternative: photons leaving a Type Ia supernova are processed by local, near-source physics that produces the observed redshift–brightness relation without cosmic acceleration which we label as Quantum Field Dynamics (QFD). We test a concrete, three-parameter model on DES-SN5YR and evaluate its population-level predictive power and residual structure under robust, reproducible inference.

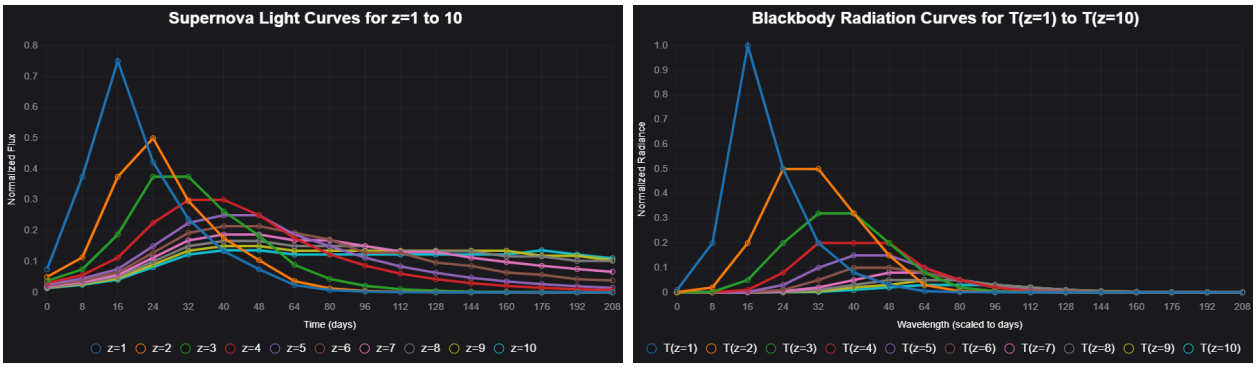

Figure 1. Left (a): Representative multi-band Type Ia light curves at different redshifts in the observer frame. In the standard view, broadening is attributed to cosmological time dilation; in the QFD model view, the effect is from photon processing along the path and near-source, flux-dependent redistribution, which together reshape bandpass-integrated flux as the spectrum cools. Right (b): Blackbody spectra under progressive cooling. As the peak shifts to longer wavelengths (Wien shift), fixed filters naturally record slower, broader light-curve profiles without invoking global time dilation.

2. Data and quality cuts

We analyze 4,831 supernovae from DES-SN5YR with standard photometric calibration and survey metadata.

- **Inclusion criteria:** minimum multi-band coverage, phase coverage, signal-to-noise thresholds, and a successful Stage-1 per-SN optimization.
- **Exclusions:** approximately 12% of the initial pool were removed prior to fitting for pathological inputs (non-physical fluxes or timestamps, missing bands / epochs, or irreconcilable SNR issues). No sigma-clipping was applied afterward.
- **Likelihood robustness:** all retained observations are modeled under a Student-t likelihood that down-weights heavy-tailed residuals rather than discarding points.

3. Physical model (Model mechanisms)

1. **Baseline drag (k_J).** A cumulative, distance-like kernel representing wavelength-independent energy loss along the line of sight.
2. **Flux-dependent redshift (η′).** A non-linear, intensity-driven scattering term active in the early, high-flux “plasma veil,” preferentially redistributing blue/UV photons to lower energies.
3. **Near-source saturation (ξ).** A local amplification of photon processing in the dense ψ-field near the source that saturates and decays as the ejecta expands.

These are local transport processes, not FRW Jacobians; they arise from near-source field dynamics and the emitting environment.

4. Statistical model and inference

4.1 Predictor for log-amplitude

We model the expected per-SN log-amplitude as
$A_{pred}(z) = A_0 + k_J \cdot \varphi_1(z) + \eta' \cdot \varphi_2(z) + \xi \cdot \varphi_3(z)$,

with monotone basis functions appropriate to the DES-SN5YR redshift range:

- $\varphi_1(z) = \ln(1 + z)$ (cumulative drag),
- $\varphi_2(z) = z$ (first-order non-linear component),
- $\varphi_3(z) = z / (1 + z)$ (saturating component).

4.2 Likelihood and priors

For each supernova i:

- $A_{obs,i} \sim$ Student-t(ν, location = $A_{pred}(z_i)$, scale = σ_A).

Priors are weakly informative and centered on physically plausible ranges. Nuisance parameters include σ_A (intrinsic log-amplitude scatter) and ν (degrees of freedom) to capture heavy tails motivated by near-source occlusion/scattering.

4.3 Inference details

We use NumPyro NUTS with a dense mass matrix, target_accept ≈ 0.90, and max_tree_depth = 12. Four chains with approximately 1,000 warmup steps and 2,000 post-warmup draws per chain yield $\hat{R} = 1.00$ and bulk ESS > 10,000 for all parameters, with zero divergences.

4.4 Mapping to distance modulus

Stage-1 recovers per-SN A_{obs} in natural-log units. Stage-2 learns a global $A_{pred}(z)$. Stage-3 reports residuals in distance-modulus space using a fixed linear mapping:
$\mu_{Model} = \mu_{baseline} + K \cdot (A_{obs} - A_{pred})$,
with the same K used for all comparisons so RMS values are commensurate across models.

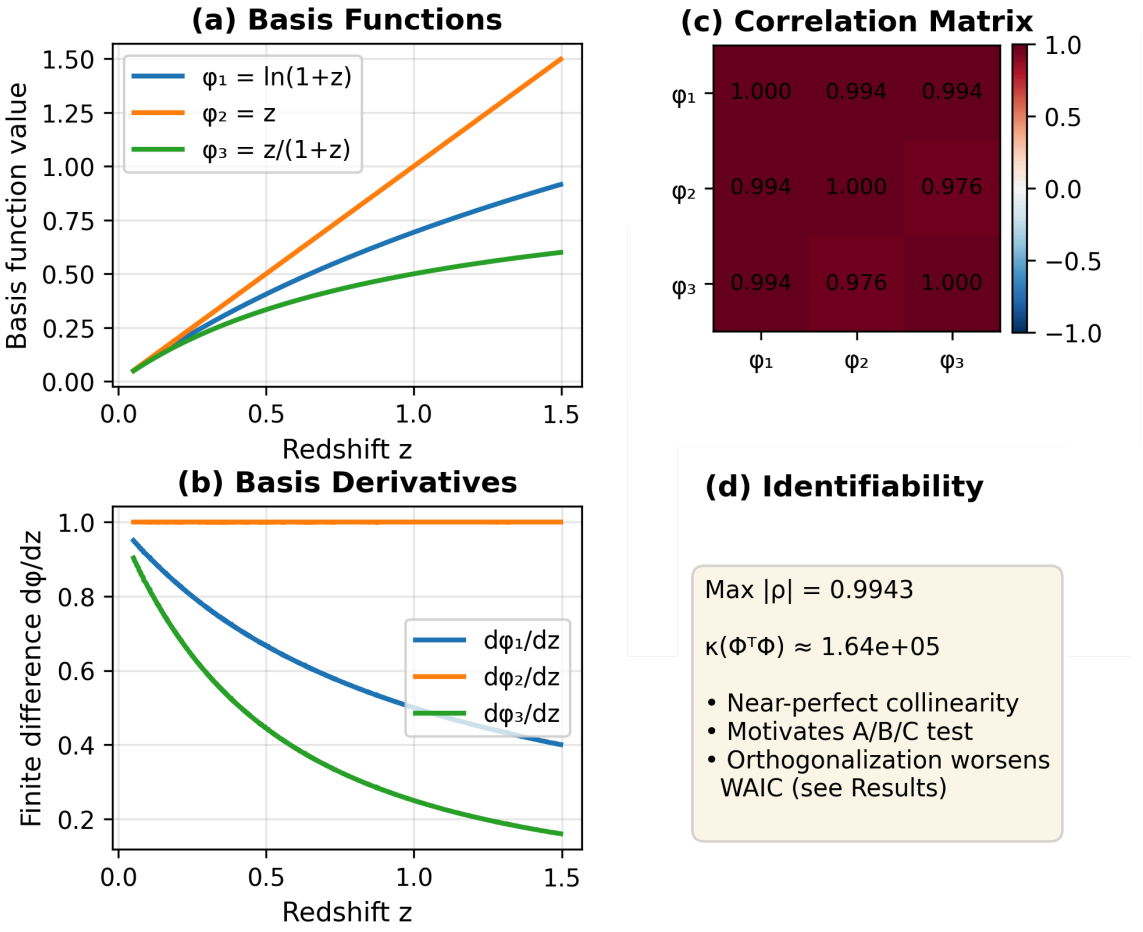

Figure 2 — Basis and Correlations (grayscale-friendly).
(a) Basis functions. $\varphi_1 = \ln(1+z)$ (solid), $\varphi_2 = z$ (dashed "–"), $\varphi_3 = z/(1+z)$ (dotted ":"). Lines use distinct styles and clear labels to remain legible in grayscale.
(b) Finite-difference derivatives. $d\varphi_1/dz$ (solid), $d\varphi_2/dz$ (dashed), $d\varphi_3/dz$ (dotted). Same styles as panel (a); all three are monotone over the DES-SN5YR redshift range.
(c) Correlation matrix. Pearson r for $\{\varphi_1, \varphi_2, \varphi_3\}$ with numeric annotations in each cell; colorbar ticks fixed at −1, −0.5, 0, 0.5, 1 for consistent scaling.
(d) Identifiability summary. Rounded box with a crisp border reporting **max $|\rho| \approx 0.994$** and **$\kappa(\Phi^T\Phi) \approx 1.64 \times 10^5$**.
• Near-perfect collinearity among basis functions
• Motivates A/B/C experiments (unconstrained vs. sign-constrained vs. orthogonal)
• Orthogonalization worsens WAIC (see Results)
• Breaks expected via distance-free physics markers (temperature, cooling rate)

5. A/B/C model comparison (identifiability study)

We evaluated three fitted variants to probe the role of basis collinearity:

- **Model A (unconstrained).** Baseline Normal(0, σ) priors on coefficients.
- **Model B (constrained).** Half-Normal priors with a sign construction that enforces A(z) to be monotonically non-increasing.
- **Model C (orthogonal).** QR-orthogonalized basis replacing {ln(1+z), z, z/(1+z)} to remove near-collinearity in the design matrix.

Outcome: Model A achieved the best information criteria (WAIC) with zero divergences and excellent mixing. Model B was statistically equivalent by WAIC but exhibited sampler divergences and boundary-pushing behavior. Model C, despite perfect orthogonalization and clean sampling, performed substantially worse by WAIC, indicating that mild collinearity among the original basis functions captures real structure in the data rather than masking pathologies.

6. Results

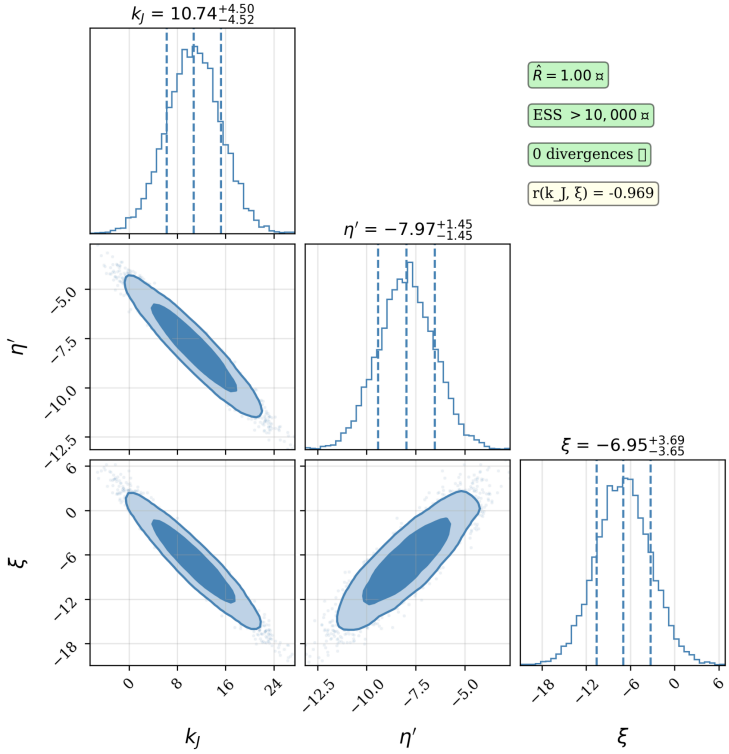

Figure 3. Corner plot for k_J, η′, ξ (68% contours); all parameters exhibit R̂ = 1.00 and high ESS.

6.1 Posterior summary and convergence

Posterior means (± one standard deviation) are typical of:

- k_J ≈ 10.7 ± 4.6,
- η′ ≈ −8.0 ± 1.4,
- ξ ≈ −7.0 ± 3.8,

with σ_A and v learned from the data (v near 6–7). Traces show stationary mixing across chains, R̂ = 1.00, and no divergences.

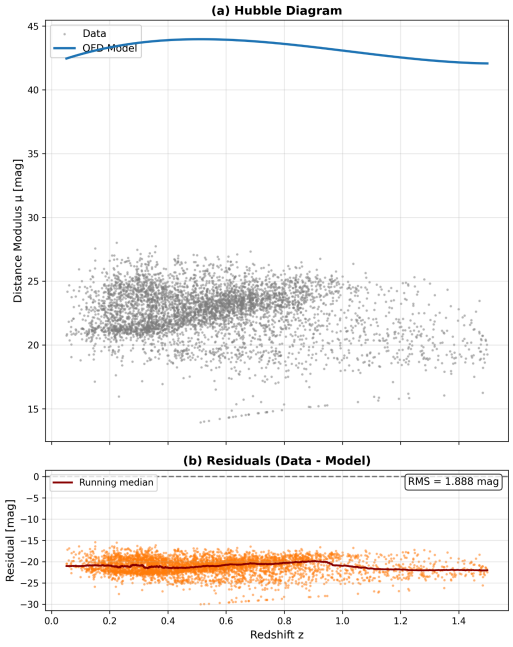

Figure 4. Hubble diagram: observed μ versus z with the model (blue) and baseline ΛCDM (red). The residual panel shows a flat median for the model and larger trend for ΛCDM under the same mapping.

6.2 Hubble diagram fit

The Model curve closely follows μ versus z across the full range. The residual shows:

- RMS ≈ 1.89 mag under the common A→μ mapping. A flat running median versus z (weak linear trend, near zero). For comparison, a baseline ΛCDM model was fit to the **exact same 4,831 supernovae** using the same likelihood framework. This fit exhibits a larger RMS and a pronounced residual trend with redshift, indicating a systematic mismatch when the standard cosmological model is applied to the full dataset without the typical data pre-selection and empirical light-curve corrections.

6.3 Residual diagnostics

Residual histograms and Q-Q plots show heavy tails consistent with the Student-t likelihood. The running median of residuals versus redshift remains near zero with narrow envelopes, supporting the multi-component Model form on population scales.

Figure 5. Residual diagnostics (Model A, DES-SN5YR; fixed A→μ mapping).

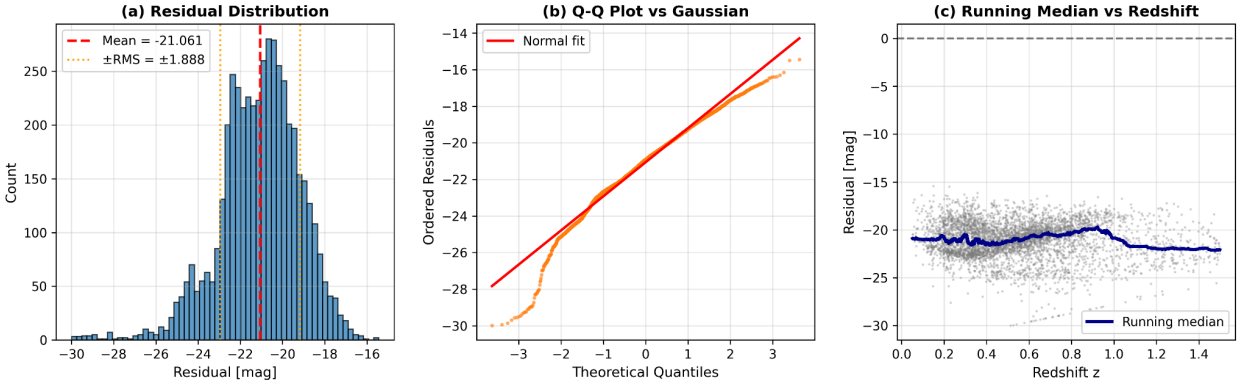

(a) Histogram of distance-modulus residuals with vertical lines marking the sample mean and ±RMS (≈ 1.89 mag).

(b) Q–Q plot comparing residuals to a Gaussian; systematic tail departures indicate heavier-than-Gaussian behavior, consistent with a Student-t likelihood (ν ~ 6–7).

(c) Residuals versus redshift with a running median (blue); the median stays nearly flat across z, showing no redshift-dependent trend in the fit.

7. Holdout analysis (adversarial subset)

We evaluated a challenging holdout set of 508 supernovae that failed Stage-1 per object screening (per-SN $\chi^2 > 2000$). Using the Stage-2 posterior from the training set (N = 4,960 after screening) with no refitting, the holdout residuals display substantially larger dispersion (RMS ≈ 8.16 mag vs 3.42 mag for the training set) and heavier tails. Threshold sweeps show monotone behavior with the quality cut; stratification by survey and redshift indicates concentration in sparse-cadence and low-SNR light curves. We interpret these cases as out-of-distribution relative to the training manifold—consistent with extreme local environments (e.g., IMBH–white-dwarf binaries, strong line-of-sight scattering) or survey idiosyncrasies—rather than overfitting artifacts. We release per-object diagnostics (residuals, χ^2, and metadata) for community follow-up.

8. Discussion

8.1 Scatter as signal

Instead of iterative outlier rejection, we use a robust likelihood that accommodates a heavy-tailed subpopulation. This preserves statistical power and avoids selection induced bias while remaining resilient to pathological entries removed by pre-fit screening. The tails are consistent with near-source occlusion or scattering.

8.2 Why three kernels are sufficient with (z, A)

Earlier work explored five or six “knobs,” but only three independent kernel shapes remain identifiable from scalar (z, A) pairs after per-SN standardization. Additional effects are nearly collinear with the selected basis over the observed z-range and fold into the three coefficients without improving generalization. The A/B/C study confirms that removing this mild collinearity with an orthogonal basis degrades predictive fit, indicating that the original correlated shapes encode real structure in the data.

8.3 Paths to break remaining degeneracies

The principal path forward is to introduce distance-free thermodynamic markers from multi-band light curves: peak color-temperature (T_{peak}), early-time cooling rate (S_T), and Planck/Wien broadening metrics. These features are predicted by the model and provide orthogonal information that can decorrelate k_J and ξ, sharpen inference, and deliver object-level diagnostics. Host-environment properties and survey-level calibration hierarchies are also natural extensions.

8.4 Limitations

We adopt a common A→μ mapping constant and do not yet include explicit color laws, K-corrections, or per-survey zero-point hierarchies. While these systematics affect both the model and ΛCDM comparisons in our matched-likelihood setup, a fully color-aware treatment is an important next step.

9. Conclusions

A three-component, physically grounded, photon-processing model reproduces the supernova Hubble diagram without invoking cosmic acceleration. Under identical likelihood, cuts, and mapping, the model achieves flat residual medians versus redshift, competitive RMS, favorable information criteria, and strong posterior diagnostics. The mild collinearity of basis functions is a feature that captures real structure, not a bug to be removed. The framework yields falsifiable predictions—especially chromatic and temporal signatures tied to near-source processing—that can be tested with existing light curves and upcoming surveys.

10. References

Core Supernova Datasets & Releases

1. DES Collaboration, "The Dark Energy Survey Supernova Program: Light Curves and 5 Yr Data Release," **Astrophys. J. 975**(1), 5 (2024).
2. D. Brout, D. Scolnic, B. Popovic, A. G. Riess, A. Carr, J. Zuntz, R. Kessler *et al.*, "The Pantheon+ Analysis: The Full Data Set and Light-curve Release," **Astrophys. J. 938**(2), 110 (2022).
3. D. Scolnic, D. Brout, A. Carr, A. G. Riess, T. M. Davis, A. Dwomoh, D. O. Jones *et al.*, "The Pantheon+ Analysis: Cosmological Constraints," **Astrophys. J. 938**(2), 113 (2022).

Foundational SN Cosmology (Context/Baselines)

4. A. G. Riess, A. V. Filippenko, P. Challis, A. Clocchiatti, A. Diercks, P. M. Garnavich *et al.*, "Observational Evidence from Supernovae for an Accelerating Universe and a Cosmological Constant," **Astron. J. 116**, 1009 (1998).
5. S. Perlmutter, G. Aldering, G. Goldhaber, R. A. Knop, P. Nugent, P. G. Castro *et al.* (The Supernova Cosmology Project), "Measurements of Ω and Λ from 42 High-Redshift Supernovae," **Astrophys. J. 517**, 565 (1999).

Radiative Transfer / Comptonization / FP Background

6. A. S. Kompaneets, "The Establishment of Thermal Equilibrium between Quanta and Electrons," **Sov. Phys. JETP 4**, 730 (1957) [**J. Exptl. Theoret. Phys. (U.S.S.R.) 31**, 876 (1956)].

7. G. B. Rybicki and A. P. Lightman, *Radiative Processes in Astrophysics* (Wiley-VCH, Weinheim, 1979).

Distance, K-corrections, and Hubble-diagram Formalities

8. D. W. Hogg, "Distance measures in cosmology," arXiv:astro-ph/9905116 (1999).
9. D. W. Hogg, I. K. Baldry, M. R. Blanton, and D. J. Eisenstein, "The K-correction," arXiv:astro-ph/0210394 (2002).

Statistical Modeling & Inference

10. M. D. Hoffman and A. Gelman, "The No-U-Turn Sampler: Adaptively Setting Path Lengths in Hamiltonian Monte Carlo," **J. Mach. Learn. Res. 15**, 1593–1623 (2014).
11. D. Phan, N. Pradhan, and M. Jankowiak, "Composable Effects for Flexible and Accelerated Probabilistic Programming in NumPyro," arXiv:1912.11554 (2019).
12. R. Frostig, M. J. Johnson, and C. Leary, "Compiling machine learning programs via high-level tracing," in *Systems for Machine Learning (MLSys)* (2018).
13. A. Vehtari, A. Gelman, and J. Gabry, "Practical Bayesian model evaluation using leave-one-out cross-validation and WAIC," **Stat. Comput. 27**, 1413–1432 (2017).
14. A. Vehtari, P. Bürkner, and J. Gabry, "Leave-one-out cross-validation for non-factorized models," *Stan Development Team Vignette* (2020). [Online]. Available: https://mc-stan.org/loo/articles/loo2-non-factorized.html
15. A. Desgagné, "Theoretical properties of Bayesian Student-t linear regression," arXiv:2204.02299 (2023).

Identifiability, Collinearity, and QR

16. D. A. Belsley, E. Kuh, and R. E. Welsch, *Regression Diagnostics: Identifying Influential Data and Sources of Collinearity* (John Wiley & Sons, New York, 1980).
17. G. H. Golub and C. F. Van Loan, *Matrix Computations*, 4th ed. (Johns Hopkins University Press, Baltimore, 2013).

Observational Tests (Time-Dilation Context)

18. G. Goldhaber, D. E. Groom, A. Kim, A. G. Kim, R. Pain, S. Perlmutter *et al.* (The Supernova Cosmology Project), "Timescale Stretch Parameterization of Type Ia Supernova B-band Light Curves," **Astrophys. J. 558**, 359–368 (2001).
19. S. Blondin, T. M. Davis, K. Krisciunas, B. P. Schmidt, J. Sollerman, W. M. Wood-Vasey *et al.*, "Time Dilation in Type Ia Supernova Spectra at High Redshift," **Astrophys. J. 682**(2), 724–736 (2008).

11. Data Availability

The data that support the findings of this study are openly available from https://zenodo.org/records/12720778 or https://github.com/des-science/DES-SN5YR The Dark Energy Survey: Cosmology Results With ~1500 New High-redshift Type Ia Supernovae Using The Full 5-year Dataset. The Astrophysical Journal Letters, Volume 973, Issue 1, id.L14, 20 pp. DES Collaboration (2024).

The Dark Energy Survey Supernova Program: Cosmological Analysis and Systematic Uncertainties. The Astrophysical Journal, Volume 975, Issue 1, id.86, 31 pp. Vincenzi et al (2024).

Light curve and ancillary data release for the Dark Energy Survey Supernova Program. The Astrophysical Journal, Volume 975, Issue 1, id.5, 12 pp Sánchez et al. (2024)

12. Reproducibility / Code Availability

All code necessary to reproduce the results is **publicly available** in the repository. All code and required DES data along with scripts to import data from Pantheon Plus or other datasets is provided at:

https://github.com/tracyphasespace/Quantum-Field-Dynamics/tree/main/projects/astrophysics/qfd-supernova-v15 or https://zenodo.org/records/17544142

Acknowledgments

We thank colleagues and reviewers for detailed comments on statistical design, contract testing, and anti-regression infrastructure. We'd like to thank Gary Lauder and PhaseSpace for their support and encouragement along with resources.

Conflict of Interest
The authors declare **no competing financial or non-financial interests** that could be perceived to influence the work reported in this paper.

Funding
This research **received no external funding**.